Structural Analysis of Historical Constructions, New Delhi 2006
P.B. Lourenço, P. Roca, C. Modena, S. Agrawal (Eds.)

The discrete element method with 2D Rigid Polygonal and Circular Elements

G.A.F. Rouxinol
Polytechnic Institute of Viseu - School of Technology, Department of Civil Engineering, Viseu, Portugal

P. Providência
University of Coimbra, Faculty of Sciences and Technology, Dep. of Civil Eng., Coimbra, Portugal

J.V. Lemos
LNEC, Lisbon, Portugal

ABSTRACT: This work depicts an algorithm for the discrete element method (DEM) considering plane rigid elements with two types of geometry, polygonal and circular, which exhibit qualitatively distinct mathematical descriptions. This algorithm allows the computation of the collapse load, and corresponding mode, of masonry structures such as arches, whose deformability is mostly concentrated at the elements interface. The polygonal elements are used for the arch representation, and the circular elements for the supported fill material. Circular elements do not directly contribute to the bearing capacity of the structure, yet their presence increases it and they are also required to model some fill material actions such as the load transfer from the top pavement to the arch itself. The mesh generation is automatic, allowing for different types of basic entities, such as arches, columns and fill material. The collapse mode and load for the Bridgemill masonry arch bridge are compared with the corresponding observed results.

1 INTRODUCTION

In the DEM, a deformable contact model is usually adopted, Lemos (1995), where a geometric small superposition is allowed under the presence of compression forces between distinct discrete elements (DE). In the point contact model the 2D external boundary of each DE is replaced by a small number of potential contact points appropriately located, Lemos (1997), corresponding to a discretization of the surface. A contact is generated whenever one such point associated with a DE intersects the surface of a neighbouring DE, which is also represented by some of its points. For a given discretization the interaction forces developed at the contact points depend of the interpenetration of the contacting DE.

The constitutive models for the interface can be formulated in terms of stresses or of the resulting forces, Pires and Costa (1989). The stress formulation is used when it is required (i) a precise evaluation of the stresses, such as in the case of large discontinuities in rocks, or (ii) the displacement history. In the particular case of circular discrete elements (CDE) the Hertz-Mindlin contact model is suitable, ITASCA (2002). The force formulation is simpler and can be adopted for the determination of the collapse load of a structure because the local deformability is not critical for the determination of the collapse mechanism. Also, from the numerical standpoint, the force formulation avoids the singularities associated with sudden stiffness variations due to changes in the contact type. Also, when small CDE are considered as a fill material, the force formulation is more efficient, and the normal stiffness of the contact can be considered as a penalty factor.

In the DEM the contact stiffness represents the total deformability of the system (i.e. deformability of both the DE and the joints before the collapse of the structure) and it may be obtained with lab tests (Lemos 1990, Vieira 1997).

This communication aims at illustrating the use of the DEM with 2D polygonal (PDE) and circular rigid DE to determine the collapse mode and load of masonry structures.

2 CONTACT REPRESENTATION

For 2D analysis the mechanical interaction model at the contact points consists of a normal spring and a shear spring. The interaction forces are function of the relative displacements, i.e., deformation of these springs and of their stiffness.

A simple and systematic definition of the contacts is required in order to guaranty the consistency of the geometrical relations as well as the efficiency of the contact detection method. For instance, the replacement of the corners of the PDE boundary by circular arcs allows for an univocal definition of the contact.

2.1 Contact definition

In the 2D case seven data items are required for the complete characterization of each contact: (i) the contact label C_i (i = 1, …, number of contacts); (ii) the contact type T_i; (iii) the contact point coordinates $\boldsymbol{x}_i^C \equiv x_{i,j}^C$ (j = 1, 2); (iv) the contact surfaces normal $\boldsymbol{n}_i^C \equiv n_{i,j}^C$, see Eq. (1); (v) the labels of the interacting DE $K_{i,m} = \{K_{i,1}, K_{i,2}\}$, ($K_{i,1} < K_{i,2}$); (vi) the coordinates $\boldsymbol{x}_{i,m} \equiv x_{i,m,j}$ of the centres of mass of the interacting DE; (vii) the coordinates of the vertices $\boldsymbol{x}^{\Upsilon}_{i,m} \equiv x^{\Upsilon}_{i,m,j}$ and of the theoretical vertices $\boldsymbol{x}^{\Upsilon T}_{i,m} \equiv x^{\Upsilon T}_{i,m,j}$. ($i$, m and j denote, respectively, contact, DE and coordinate. When the reference contact is evident the first of these subscripts may be dropped.)

A PDE vertex (corner) is represented by the symbol Υ. In the model adopted the sharp vertices are replaced by circular regions whose centre is located at the theoretic corner represented by Υ^T. This circular arc which "smoothes" the corner has radius R and defines the rounding distance d_r from the geometric vertex to each of the two tangency points with the straight edges.

In order to optimize the use of the contact detection subroutines a contact is created before physical or effective contact occurs, and named *virtual* contact. Contact forces are produced only for *real* contacts, corresponding to effective superposition of the interacting DE. In each iteration most of the quantities characterizing each contact are updated. For the contact C_i a local rectangular coordinate system $(t,n)_i^C$ is defined, with origin at the contact point and axes parallel to the contact tangent and normal at that point, as given by the directions

$$\overline{\boldsymbol{n}}_i^C = \left[\boldsymbol{t}_i^C \;\middle|\; \boldsymbol{n}_i^C \right] = \left[\begin{array}{c|c} n_{i,2} & n_{i,1} \\ -n_{i,1} & n_{i,2} \end{array} \right] \tag{1}$$

where $n_{i,1}$ and $n_{i,2}$ are the normal coordinates in the global coordinate system, see Fig. 1. The positive direction of the normal is from $K_{i,1}$ to $K_{i,2}$.

There are eight different contact types T_i: (1) corner-corner; (2) corner-edge; (3) edge-corner; (4) circle-circle; (5) corner-circle; (6) edge-circle; (7) circle-corner; (8) circle-edge, where the terms corner and edge are used for PDE and the term circle for CDE. As an example, in Fig. 1 contacts C_i, i = 1, 2, 3 and 4 are of types 4, 7, 8 and 3, respectively. The normal direction of the local coordinate system is perpendicular to the edge for cases 2, 3, 6 and 8; and connects the real and/or theoretical corners in the remaining cases. The normal axis contains always at least a real and/or theoretical centre. The origin of the local coordinate system is located (on this axis) at the middle of the segment connecting the two DE.

The contact classification requires the verification of specific geometric conditions. For a contact of type 1, there are two corners potentially in contact, Υ_i and Υ_{i+k}. In this case the conditions are: (i) the projection of the theoretic vertex Υ^T_i on the edges adjacent to Υ_{i+k} must fall inside the circular region and vice versa; (ii) the PDE superposition d^C (a negative value meaning effective superposition) must satisfy two admissible tolerances $d_O > 0$ and $d_G > 0$, the first one controlling effective contact and the second effective separation,

$$-d_O < d^C < d_G \quad \text{where} \quad d^C = \overline{\Upsilon_i^T \Upsilon_{i+k}^T} - R_i - R_{i+k} \tag{2}$$

For contacts of types 4, 5 and 7 the criteria are similar to those above, but simpler as it may be unnecessary to verify if the contact occurs in a circular region.

For contacts of types 2, 3, 6 and 8 similar geometric conditions apply. For instance, let's consider a type 3 contact (like C_4, on Fig. 1) and the local frame of reference $(t,n)_i^C$. The points of

$K_{i,1}$ where its circular regions join its straight edge must have abscissas with opposite signs. The contact condition must also be satisfied, with the superposition given in this case by $d^C = D - R_i$, where D is the distance from the edge to the theoretic centre Υ^T_i.

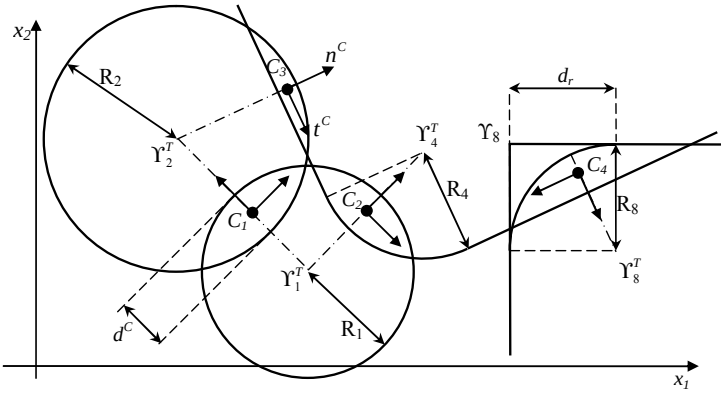

Figure 1: Representation of the contacts between several discrete elements.

2.2 Contact detection

One critical aspect of the DEM is the automatic recognition of new contact states and the removal of those that lost pertinence, as the process evolutes. This requires a simple representation of the potential contact zones as well as robust and efficient algorithms to detect/update them during the analysis (Cundall 1988, Lemos 1999, Munjiza 2004).

Cundall's method and the enveloping volumes method, Williams (1988), were adopted at a lower level. Cundall´s method partitions the set of DE over a rectangular reticulate mesh (top of Fig. 2), and attributes to each of its cells the DE and the contacts that fall inside its domain. This replaces the direct search over the whole domain by a search in each individual cell thus reducing significantly the CPU time consummation.

At a higher level the enveloping volumes method, which breaks off the contact detection process for any two elements reasonably away one from the other, was adopted for the search inside each cell. More advanced methods such as binary trees could be used but they are particularly appropriate for 3D systems or for the simulation of CDE systems flow.

3 DISCRETE ELEMENT EQUATIONS

The developed DEM algorithm aims at the analysis of systems containing both polygonal and circular discrete elements. The method formulation is well established, being based on Newton's second law for the DE centres of mass displacements and a constitutive force-displacements relation at the contact level, as a function of those displacements, Cundall and Strack (1979). The DE are considered rigid and a point deformability model is adopted for the joints, which accounts for the whole system deformation.

3.1 Force displacement law

For each real contact state ($d^C < 0$) there is a pair of compression normal forces and a pair of shear forces, which are function of the normal and shear components of the displacement at the contact and of its stiffness. At the contact C_i the relative velocity in the main coordinate system is given by $\dot{\boldsymbol{u}}_i^C = \dot{\boldsymbol{u}}_{i,2}^C - \dot{\boldsymbol{u}}_{i,1}^C$, where $\dot{\boldsymbol{u}}_{i,m}^C \equiv \dot{u}_{i,m,j}^C$, $j = 1,2$, is the velocity at the contact of the discrete element $K_{i,m}$ with components

$$\dot{u}_{i,m,j}^C = \dot{u}_{i,m,j} - e_{jk3} w_{i,m} (x_{i,k}^C - x_{i,m,k}), \quad j,k = 1,2 \tag{3}$$

where $\dot{u}_{i,m,j}$ and $w_{i,m}$ are the centre of mass velocity j-component and angular velocity (measured counterclockwise) of element $K_{i,m}$, and e_{jk3} is the permutation symbol. In the case of the corners of PDE the determination of this velocity can be approximated by the velocity of the geometric vertex, eq. (13). The shear and normal components of the relative velocity are

$$\begin{Bmatrix} \dot{u}_s^C \\ \dot{u}_n^C \end{Bmatrix} \equiv \begin{Bmatrix} \dot{u}_{i,s}^C \\ \dot{u}_{i,n}^C \end{Bmatrix} = \left(\overline{\boldsymbol{n}}_i^C\right)^t \begin{Bmatrix} \dot{u}_{i,1}^C \\ \dot{u}_{i,2}^C \end{Bmatrix} \tag{4}$$

so that the contact displacement increments during the time step Δt are approximately given by

$$\begin{Bmatrix} \Delta u_s^C \\ \Delta u_n^C \end{Bmatrix} = \begin{Bmatrix} \dot{u}_s^C \\ \dot{u}_n^C \end{Bmatrix} \times \Delta t \tag{5}$$

and, as a first approximation, the corresponding contact shear and normal forces increments are

$$\begin{Bmatrix} \Delta F_s^C \\ \Delta F_n^C \end{Bmatrix} = -\begin{bmatrix} k_s & 0 \\ 0 & k_n \end{bmatrix} \begin{Bmatrix} \Delta u_s^C \\ \Delta u_n^C \end{Bmatrix} \tag{6}$$

(normal force positive in compression), where k_n and k_s are the linear stiffness for the contact C_i. Assuming that the time step is small enough, the magnitude of the rotation at the contact will also be sufficiently small to allow for the computation of the total contact normal and shear forces from the simple sum

$$\begin{Bmatrix} F_n^C \\ F_s^C \end{Bmatrix}^* = \begin{Bmatrix} \Delta F_n^C \\ \Delta F_s^C \end{Bmatrix} + \begin{Bmatrix} F_n^C \\ F_s^C \end{Bmatrix} \tag{7}$$

where the asterisk means that these total values must still satisfy the failure criteria: (i) no tension (i.e. if $F_n^{C*} < 0$ the contact is eliminated together with the contact forces, F_s^C, $F_n^C \rightarrow 0$); (ii) maximum compression equal to the DE material strength, and (iii) maximum shear force defined by the Mohr-Coulomb failure criterion, $F_s^{\max} = c + F_n^C \tan\phi$, where c and ϕ are the joints cohesion and angle of friction. If (7) gives $|F_s^{C*}| > F_s^{max}$ then the effective magnitude is

$$F_s^C = F_s^{max} \times F_s^{C*} \Big/ \left|F_s^{C*}\right| \tag{8}$$

The statically equivalent forces and moments at the centre of mass of each of the two contacting DE are computed from the contact forces. For instance, for the contact C_i between DE $K_{i,m}$, $m = 1,2$, they are given by (feel free to ignore the subscripts i and m to increase legibility)

$$\begin{cases} F_{i,m,j} = F_{i,m,j}^C \\ F_{i,m,3} = e_{kl3}(x_{i,k}^C - x_{i,m,k}) F_{i,m,l}^C \end{cases}, \quad j,k,l = 1,2, \quad \begin{Bmatrix} F_{i,m,1}^C \\ F_{i,m,2}^C \end{Bmatrix} = (-1)^m \left(\overline{\boldsymbol{n}}_i^C\right) \begin{Bmatrix} F_{i,m,s}^C \\ F_{i,m,n}^C \end{Bmatrix} \tag{9}$$

3.2 Law of motion

Newton's second law and its rotational version define the movement for each rigid DE,

$$\begin{cases} F_j = m\,\ddot{u}_j \\ F_3 = I_m \dot{w} \end{cases}, \quad j = 1,2 \tag{10}$$

with forces and displacements referred to the element centre of mass, m is the mass, I_m the mass moment of inertia and $\dot{w}$ the rotational acceleration. For a quasi-static analysis the consideration of numerical damping produces energy dissipation and allows the convergence to an equilibrium state (or a collapse mode) in a finite number of iterations. A global viscous damping is defined as a speed proportional force, $F_i^D = D\,\dot{u}_i$, where the mass proportional damping coeffi-

cient is given by $D = \alpha m$. Using the finite difference method with the central difference scheme to integrate (10), with a time step Δt, gives the velocity at time $t + \Delta t/2$

$$\begin{cases} \dot{u}_j^{t+\Delta t/2} = \left(\dot{u}_i^{t-\Delta t/2} D_1 + \beta_1 F_j^t\right) D_2 \quad , \quad j = 1,2 \\ w^{t+\Delta t/2} = \left(w^{t-\Delta t/2} D_1 + \beta_2 F_3^t\right) D_2 \end{cases} \tag{11}$$

with $\beta_1 = \Delta t / m$, $\beta_2 = \Delta t / I_m$, $D_1 = 1 - \alpha \Delta t / 2$ and $D_2 = 1 / (1 + \alpha \Delta t / 2)$. The centre of mass new displacement components are given by

$$\begin{cases} u_j^{t+\Delta t} = u_j^t + \dot{u}_j^{t+\Delta t/2} \Delta t \quad , \quad j = 1,2 \\ \theta^{t+\Delta t} = \theta^t + w^{t+\Delta t/2} \Delta t \end{cases} \tag{12}$$

For the PDE the corner velocity and displacement components are given by

$$\begin{cases} \dot{u}_j^{r,t+\Delta t/2} = \dot{u}_j^{t+\Delta t/2} - e_{jk3} w^{t+\Delta t/2} (x_k^{r,t} - x_k^t) \\ u_j^{r,t+\Delta t} = u_j^{r,t} + \dot{u}_j^{r,t+\Delta t/2} \Delta t \end{cases}, \quad j,k = 1,2 \tag{13}$$

The magnitude of the selected time step Δt is a critical factor because the computational cost is proportional to the total number of time steps required to achieve a resting state of the structural system. The stability of the recurrent numerical operator and the accuracy of the integration are the two main factors to consider when seeking for the maximum allowed value for Δt. For stability the spectral radius of the recurrent operator must be smaller than the unity. For the direct integration of (10) and in order to satisfy the last condition, the conditionally stable central difference scheme requires a time step which satisfies, Bathe (1982),

$$\Delta t \le \Delta t_{cr} = T_{min} / \pi \,, \tag{14}$$

where T_{min} is the minimum non damped period of the DE system. The code developed includes also the capability to perform an eigenvalue analysis, under the assumption of elastic joints, which allows the confirmation of the simplified formulas adopted in practice. In general the integration accuracy will also be verified if Δt satisfies (14). By considering a regular mesh and a unique DOF global mode with maximum relative displacement at the contacts, Morikawa et al. (1993), one obtains a simplified expression for T_{min} which gives

$$\Delta t_{cr} = 2\varphi \sqrt{m_{min} / k_{max}} \tag{15}$$

where the parameter $\varphi \in]0,1[$ accounts for a number of contacts larger than one (in general, use $\varphi \in]0.1,0.5[$), m_{mim} is the minimum DE mass and k_{max} is the maximum contact stiffness.

4 SYSTEM GENERATION

The characterization of the geometry of existing masonry structures can be performed by different methods, either classical, based on reading drawings and/or on measuring through tape, tachometer and laser distance meter; either more recent ones, based on photographic techniques, Costa (2002), usually designated by remote sensing (photogrammetry), in situ tests and ultrasounds, Komeyli-Birjandi (1986). In accordance to these different methods for the geometry characterization, some algorithms were developed for the conversion of AUTOCAD DXF files and the automatic generation of several types of structural elements.

The programs available for conversion of data from a DXF file into a mesh description for a finite element analysis (FEA) are inadequate for a discrete element analysis (DEA). For instance, in a FEA a vertex can join, say, four distinct DE. For the DEA this vertex is replaced by four distinct vertices, with identical coordinates, matching four distinct DE.

The developed computational procedure generates automatically several standard structural elements, allowing for the complete establishment of complete simplified models containing

large numbers of DE (say 15000). The standard structural elements include semi-circular arches, segmental (shallow/deep) arches, columns and the fill material.

Several methods are used for the generation of a irregular system of CDE simulating the arch fill material. The radius expansion method, ITASCA (2002), provides different possibilities depending on the required type of spatial particle distribution. The original method was intended mainly for systems containing only CDE and for the fill material of rectangular or circular domains. For the present work the method had to be improved because masonry arches include complex, non-convex, filling sub-domains, per instance above the circular extrados or below the pavement, which usually has a non zero inclination. In this improvement one must first define convex domains (rectangles, trapezoids, circle segments, etc., see top of Fig. 2) with a shape similar to the regions where there should be *no* DE, thus creating a kind of negative mask. Afterwards the CDE are distributed using a conventional random process for both the position and the discrete size, with criteria which will guaranty a specified porosity, see bottom of Fig. 2. After the distribution / expansion stages the weight of the fill material is "turned on" and the structural system goes through a cycle of equilibrium iterations until it comes to a still. Only then is the live-load introduced in an incremental form, each increment of the load being associated to an independent equilibrium iterations cycle.

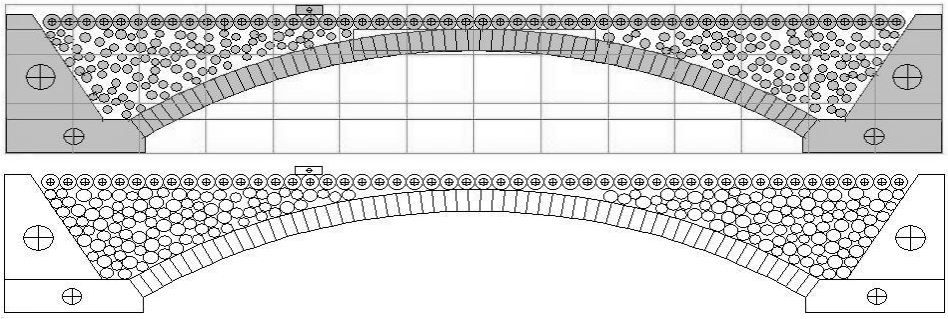

Figure 2 : Top) Unacceptable sub-domains for the CDE (gray) and rectangular reticulated mesh, Bottom) distribution of the CDE after the radius expansion stage.

5 NUMERICAL EXAMPLE

As an application of this algorithm, we consider the renowned Bridgemill masonry arch bridge at Girvan, Scotland, built in 1869. Hendry, Davies and Royles measured its geometry, determined its mechanical properties, performed a load test and registered the value of the load previous to its collapse, Page (1993). Due to the shortage of records of this nature, this example has been used by several researchers in order to validate their numerical models, Molins (1998).

The bridge arch is parabolic with a free span of 18.29 m, 8.3 m width, 2.84 m rise at midspan and it is made of 62 sandstone voussoirs, with a 71.1 cm depth. For this span/rise ratio the parabola is quite flat, almost coincident with a circular arc, so that it is admitted as a segmental arch, Page (1993). The distance from the keystone extrados to the pavement surface is 47.8 cm, including the depth of fill at crown (20.3 cm), the sub-base thickness (12.5 cm) and the bituminous surfacing (15.0 cm). The voussoirs and the spandrel walls have a density of 2100 kg/m^3, a deformation modulus of 5000 MPa and a compressive strength between 5.0 and 7.0 MPa. The fill material, composed from a mixture of gravel, sand and clay, has a density of 1890 kg/m^3 and a deformation modulus of 40 MPa.

For a "line" load 75 cm wide, crossing the whole bridge width, applied at quarter span, the registered ultimate load (not the bridge collapse load, even though it allowed the observation of the four "hinges" corresponding to the usual asymmetric mechanism) was 3100 kN.

In order to quantify the contribution of the fill material presence to the bridge overall load-carrying capacity, four distinct arrangements were analysed: (i) the isolated arch with neither the fill nor its action on the arch; (ii) the isolated arch with vertical loads simulating the fill action on the arch; (iii) the combined effect of the arch plus the fill simulated by CDE and (iv) the

combined effect of the arch plus the brickwork spandrel wall. As there is no record of the dimensions of the bricks actually used, we adopted 30×22×20 cm (rather unusual, it must be stated). Even though the analysis is, in fact, 2D, the arch width is taken 8.3 m for the four cases. Nevertheless, in what concerns the collapse load, the values per metre width are also given.

Next follows the relevant data used in the numerical modelling. For the fill we employed CDE with four distinct radii: 23.93; 14.96, 13.47 and 11.97 cm. Smaller dimensions, in particular with any specified distribution, could have been used. The contact stiffness K for PDE interaction is 5580 MN/m (K = EA/L where A is the influence area of the point contact, A = 71.1/2×100 cm^2 and L is the distance between the centres of mass of contiguous PDE, L = 31.88 cm); for CDE interaction is 40 MN/m (K = E×D/D, where D is the CDE diameter); and for PDE-CDE interaction the last value was also adopted. As there is no record of the fill internal friction angle, a value of $\phi = 35^{\circ}$ was adopted. Also for the cohesion between CDE a value of c = 100 kPa was adopted (c = 0 for the other contact types). For the live-load on the pavement a 26°load dispersion angle was used (corresponding to a 2:1 vertical to horizontal slope). The live-load is incremented until collapse in 200 kN steps (i.e. 24.096 kN per metre width), so that the given collapse load values correspond to an accuracy error of ±100 kN.

Case (i) gives a collapse load of 1700 kN (i.e. 204.8 kN/m), corresponding to stresses below the material compressive strength. Fig. 3 shows the collapse mechanism.

For case (ii) collapse occurs for a load of 2900 kN (349.4 kN/m) which demonstrates the favourable effect of fill presence. The collapse configuration is similar to that of Fig. 3.

The collapse load for case (iii) is equal to case (ii). Fig. 4 shows the bridge configuration after the collapse load was attained. Even though the vertical displacement of the voussoir located at quarter span is linear up to a load value of 2600 kN, the "line" load displacement is rather irregular due to the rearranging of the CDE under their self weight. This load-displacement local behaviour is not our present main concern, a detailed description will be given elsewhere.

For case (iv) the ultimate load reaches 3700 kN (445.8 kN / m), with a collapse mode similar to the preceding ones, Fig. 5.

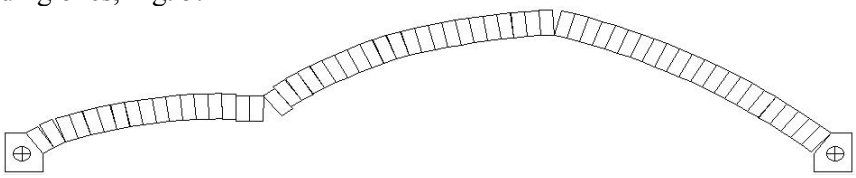

Figure 3 : Case (i) - Collapse mode of the Bridgemill bridge arch without fill for "line" live-load.

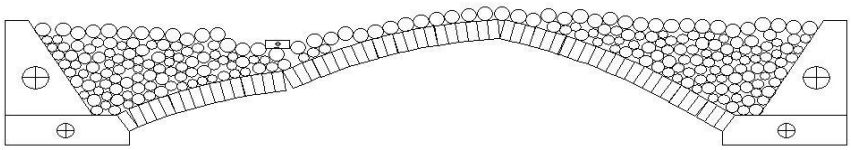

Figure 4 : Collapse mode of the arch with fill due to "line" live-load.

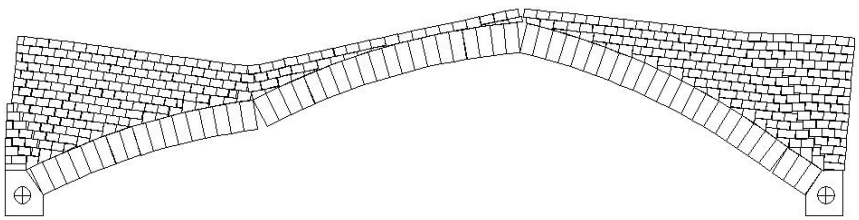

Figure 5 : Collapse mode of Bridgemill bridge arch with spandrel wall due to "line" live-load.

The overall (3D) strength of the bridge can be approximated, considering the collaboration of modes (iii) and (iv), by combining the corresponding results. This combination can be made taking into account their relative stiffnesses or, for simplicity, proportionally to their relative widths (fill 786 cm and spandrel wall 44 cm), furnishing 2940 kN, which gives a relative error of 5% when compared with the value measured in situ (in fact, we cannot state that the solution has such a accuracy, due to the magnitude of the chosen load step, as explained above).

6 CONCLUSIONS

The DEM has been acquiring an increasing significance as an analysis / project tool in structural engineering. Not only the assessment, restoration, rehabilitation, conservation and preservation of antique buildings with masonry structures, require more appropriate methods, which approximate more accurately their behaviour, allow for an improved safety evaluation and, therefore, for the development of more appropriate intervention solutions, but also the computers processors capacity persisting boost makes that possible.

In this communication we adapt the classical formulation of the DEM for systems containing rigid polygonal and circular elements. This algorithm allows, for example, to assess the effect of the fill material on the ultimate load of masonry arch bridges.

The included example of the Bridgemill masonry arch bridge illustrates the application of this algorithm. Four different situations with respect to the modelling of the fill material were treated, and both the four hinges collapse mechanism modes and the ultimate load values correspond well with the field experimental results. A more detailed report of this numerical example, including critical parameters variation influence, is under preparation.

REFERENCES

Bathe, K.J. 1982. *Finite element procedures in engineering analysis*, Prentice-Hall.

Costa, C. 2002. *Análise do Comportamento da Ponte da Lagoncinha sob a Acção do Tráfego Rodoviário*. Master´s Thesis. University of Porto, Porto.

Cundall, P.A. and Strack, O.D.L. 1979. A discrete numerical model for granular assemblies. *Géotechnique.* 29, n.1, p. 47-65.

Cundall, P.A. 1988. Formulation of three-dimensional distinct element model – Part I: A scheme to detect and represent contacts in a system composed of many polyhedral blocks. *Int. J. Rock Mech. Min. Sci. & Geomech. Abstr*. 25(3), p. 107-116.

ITASCA Consulting Group, Inc. 2002. *PFC2D – Particle Flow Code in 2 Dimensions*. User's Guide. Version 3.0. Minneapolis USA.

Komeyli-Birjandi, F. 1986. *Sonic investigation of masonry structures*. PhD Thesis. University of Edinburgh, Edinburgh.

Lemos, J.V. 1990. A comparison of numerical and physical models of a blocky medium. Rossmanith (ed.), *Mechanics of Jointed and Faulted Rock*, p. 509-514. Balkema.

Lemos, J.V. 1995. Metodologias para detecção e actualização de contactos em modelos de elementos discretos. *IV Encontro Nacional de Mecânica Computacional* 1, p. 61-72. Lisbon.

Lemos, J.V. 1997. A representação do contacto em modelos de elementos discretos. *Congresso Nacional: V Encontro Nacional de Mecânica Computacional* 1, p. 565-573. Univ. of Minho. Guimarães.

Lemos, J.V. 1999. *Modelling and failure analysis in rock engineering*. Laboratório Nacional de Engenharia Civil (LNEC), Lisbon.

Molins, C. 1998. Numerical simulation of the response of arch Bridgs. In P. Roca, J.L. González, E. Oñate and P.B. Lourenço (eds), *Structural Analysis of Historical Constructions II, Proc. Int. Seminar Barcelona, November 1998,* p. 93-123. Barcelona: CIMNE.

Morikawa, H. Sawamoto, Y. and Kobayashi, N. 1993. Local Fracture Analysis of a Reinforced Concrete Slab by the Discrete Element Method. *Proc. 2nd Int. Conf. Discrete Element Methods*, p. 275-286. Cambridge, Massachusetts IESL Publications.

Munjiza, A 2004. *The combined finite-discrete element method.* John Wiley & Sons.

Page, J. 1993. *Masonry arch bridges. State-of-the-Art Review*. Transport Research Laboratory, Department of Transport, London.

Pires E.B., e Costa P.P. 1989. Análise numérica do problema de contacto com atrito entre dois corpos elásticos. *X Congresso Ibero-Latino-Americano sobre Métodos Computacionais em Engenharia (MECOM-89)* 3 A969-A989. Porto.

Vieira J.L.M. 1997. *Um modelo de elementos discretos para o estudo de estruturas de alvenaria*. Master´s Thesis. Instituto Superior Técnico (IST-UTL). Lisbon.

Williams, J.R. 1988. Contact analysis of large numbers of interacting bodies using discrete modal methods for simulating material failure on the microscopic scale. *Eng. Computational* 5, p. 198-209.